International Journal of Multiphase Flow 85 (2016) 186–195

Contents lists available at ScienceDirect

International Journal of Multiphase Flow

journal homepage: www.elsevier.com/locate/ijmultiphaseflow

Air–water flow characteristics in high-velocity free-surface flows with 50% void fraction

Stefan Felder[a,*], Hubert Chanson[b]

[a] School of Civil and Environmental Engineering, Water Research Laboratory, UNSW Australia, 110 King Street, Manly Vale, NSW 2093, Australia
[b] School of Civil Engineering, The University of Queensland, Brisbane, QLD 4072, Australia

ARTICLE INFO

Article history:
Received 20 December 2015
Revised 9 March 2016
Accepted 6 June 2016
Available online 23 June 2016

Keywords:
High-velocity free-surface flows
Air–water time scales
Interfacial aeration
Bubble droplet interactions
Microscopic flow properties
Characteristic frequencies

ABSTRACT

High-velocity free-surface flows are complex two-phase flows and limited information is available about the interactions between air and water for void fractions of about 50%. Herein a detailed experimental study was conducted in the intermediate flow region ($C \sim 50\%$) on a stepped spillway and the microscopic air–water flow characteristics were investigated. The results showed differences in water and droplet chord times with comparatively larger number of air chord times (0–2 ms), and larger number of water chord times (2–6 ms). A monotonic decrease of particle chord modes was observed with increasing bubble count rates. Several characteristic time scales were identified based upon inter-particle arrival time analyses of characteristic chord time classes as well as spectral analyses of the instantaneous void fraction signal. Chord times of 3–5 ms appeared to be characteristic time scales of the intermediate flow region having similar time scales compared to the local correlation and integral turbulent time scales and to time scales associated with bubble break-up and turbulent velocity fluctuations. A further characteristic time scale of 100 ms was identified in a frequency analysis of instantaneous void fraction. This time scale was of the same order of magnitude as free-surface auto-correlation time scales suggesting that the air–water flow structure was affected by the free-surface fluctuations.

1. Introduction

Gas–liquid flows are a common feature in water engineering applications in chemical and mechanical engineering such as waste water treatment plants, industrial mixing processes and aeration of liquids in closed conduits (Rao and Kobus, 1971; McKeogh and Ervine, 1981; Thomas et al., 1981). In these engineering disciplines, gas–liquid flows are often characterized by single bubbles or bubble swarms surrounded by liquids in bubbly flows with average void fractions below 30% or by single liquid droplets or droplet swarms surrounded by gases with void fractions above 90%. Examples for bubbly flows include aeration in waste water treatment facilities such as membrane reactors or mixing tanks, in boiling fluids, aerated flows in pipes of various inclinations and multitude of liquids (Kobus, 1984). Spray flows with very high void fractions occur in various applications where liquids are injected into a gas phase using mechanical break-up of the liquid to increase the droplet surface in misty and spray flows (Wu et al., 1992; Crowe et al., 1998). Both bubbly and spray flows are often associated with engineered processes in industrial applications.

A different occurrence of air–water flows are gravity driven flows which can be found in water falls and drops, breaking waves and hydraulic jumps (Hoyt ad Taylor, 1976; Hoyt and Sellin, 1989; Wood, 1991; Ervine, 1998) (Fig. 1). A key feature of these naturally occurring gas–liquid flows is the existence of a range of void fractions within the air–water flow column ranging from very small void fractions furthest away from the free-surface to very high void fractions closest to the free-surface (Straub and Anderson, 1958; Ervine and Falvey, 1987). While these types of flows occur naturally, they may be observed in hydraulic structures, storm waterways and spillway systems of various slopes, and stilling basins. The air entrainment is often a key feature and linked with turbulence and boundary layer processes (Ervine, 1998). In high-velocity flows on spillways the air entrainment starts naturally at the inception point of free-surface aeration when the outer edge of the turbulent boundary layer reaches the free-surface, leading to a complex air–water flow mixture downstream (e.g. Rao and Kobus, 1971; Wood, 1991; Chanson, 1997, 2013). The aerated flows are characterized by three dimensional turbulent flow processes in the various regions of the air–water flow column (Fig. 1).

* Corresponding author. Tel.: +61280719861
E-mail addresses: s.felder@unsw.edu.au (S. Felder), h.chanson@uq.edu.au (H. Chanson).

http://dx.doi.org/10.1016/j.ijmultiphaseflow.2016.06.004
0301-9322/

(A) Stepped spillway of Paradise dam (Australia) in operation on 5 March 2013 - Flow conditions: $h = 0.62$ m, $Q \sim 2300$ m^3/s, $q \sim 7.4$ m^2/s, $d_c/h \sim 2.85$, $Re \sim 2.9 \times 10^7$

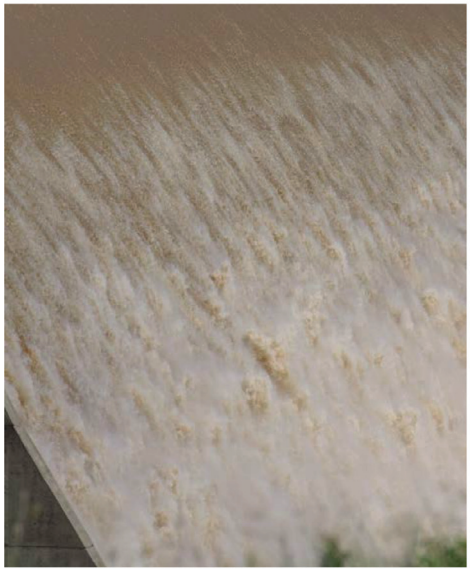

(B) Details of the upper free-surface region during the Paradise Dam spillway operation on 5 March 2013 - Flow conditions: $h = 0.62$ m, $Q \sim 2300$ m^3/s, $q \sim 7.4$ m^2/s, $d_c/h \sim 2.85$, $Re \sim 2.9 \times 10^7$

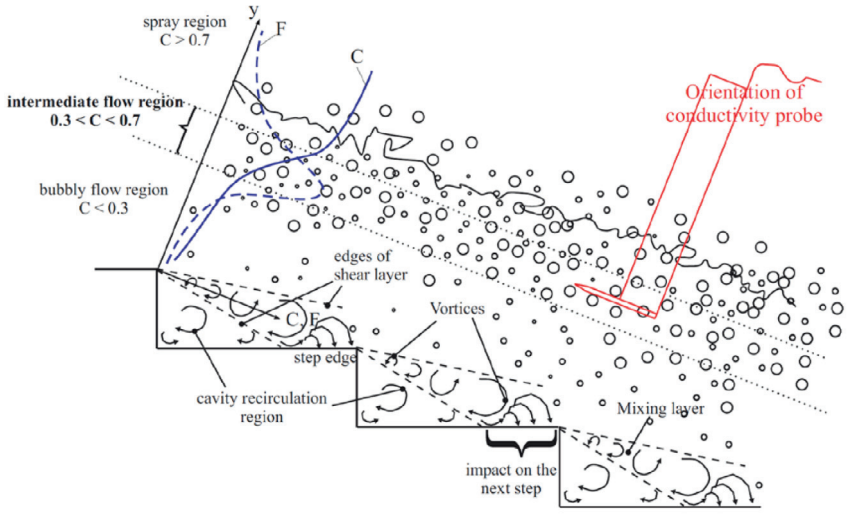

(C) Sketch of air-water flow regions in high-velocity free-surface flows on a stepped spillway; Positioning of phase-detection intrusive probe in intermediate flow region with void fraction $C = 0.5$; Sketch of typical void fraction and bubble count rate distributions

Fig. 1. High-velocity free-surface flows down a stepped spillway.

A stepped chute is a type of spillway where a significant amount of turbulent energy is dissipated in the lower water column (void fraction < 30%) in interactions with the solid boundaries including recirculation movements in the step cavities and unsteady cavity ejection processes (Chanson and Toombes, 2002). In the upper flow region, substantial ejections of water droplets in the spray region take place (void fraction > 70%) (Fig. 1). Fig. 1A presents a prototype stepped spillway in operation. Fig. 1B shows a zoom of the upper air–water flow region. The flow processes in both bubbly and spray regions are well researched with the occurrence of clearly defined air bubbles and water droplets surrounded by water and air respectively (e.g. Matos, 1999; Ohtsu et al., 2004; Felder and Chanson, 2011; Bung, 2011,2013). Similar to other bubbly and spray flows, phase detection intrusive probes and visualization techniques proved successful in characterizing bubble and droplet sizes within these flow regions.

Little information is however available on the air–water region between the bubbly and spray flow regions, i.e. the so called intermediate flow region with void fractions between about 30% and 70%. This intermediate flow region is characterized by an air–water mixture with a balanced ratio between air and water entities, by collisions, deformations, coalescence and reformations of 'bubbles' and 'droplets' . High bubble count rates, large turbulence levels and large integral turbulent scales were reported in this flow region indicating strong turbulent and energy dissipation (e.g. Chanson and Carosi, 2007; Felder and Chanson, 2011). Despite the important role of this intermediate flow region for energy dissipation and mixing processes, detailed information about the air–water flow interactions are limited.

While the intermediate flow region is typically defined between 30% < C < 70%, the present investigation focused upon void fractions C=50% +/− 1% which was considered as a canonical representation of the intermediate flow region. The void fraction is a time-averaged measure of the gas–liquid flow and hence the instantaneous representation of air–water entities within the intermediate flow region is best represented by the median, i.e. C=0.50 +/− 0.01. Herein this contribution is a first attempt for an in depths characterization of flows with equal quantity of air and water. The study provides some novel insights into the characteristic air–water time scales in a typical high-velocity flow on a stepped chute.

2. Experiments and basic results

2.1. Experimental facility and instrumentation

Experiments were conducted in a large size spillway facility comprising two stepped configurations with plywood steps of height h=5 cm or h=10 cm, respectively. The width of the facility was W=1 m, the length L=2.4 m and the slope was 1V:2H (θ=26.6°). Experiments were conducted with flow rates per unit width between 0.02 < q_w < 0.21 m^2/s corresponding to a dimensionless discharge 0.69 < d_c/h < 3.3 where d_c is the critical flow depth $d_c=(q^2/g)^{1/3}$ and to a Reynolds number defined in terms of the hydraulic diameter of 8.1 × 10^4 < Re < 5.7 × 10^5.

Air–water flow measurements were conducted with a dual-tip conductivity probe with two identical probe tips of diameter Ø=0.25 mm separated in longitudinal direction Δx=7.2 mm and transverse direction Δz=2.1 mm. At each vertical location, each sensor was sampled at a rate of 20 kHz for 45 s as suggested by Felder and Chanson (2015).

The post-processing of the raw Voltage data was conducted based upon a single-threshold technique (Cartellier and Achard, 1991) providing the time-averaged void fraction C, the bubble count rate F and the air bubble and water droplet chord times (Chanson and Toombes, 2002). A threshold of 50% was used because it was the most suitable threshold value for the various flow regions (Felder and Chanson, 2015). In further analyses, both air bubble and water droplets chords were grouped into classes of particle chord sizes for which a similar behavior may be expected (Edward and Marx, 1995) and the inter-particle arrival times were calculated. Further investigations were based upon the spectral analyses of the instantaneous void fraction signals.

The correlation analysis of the raw conductivity probe signals provided the local time-averaged interfacial velocity V, the auto- and cross-correlation integral time scale T_{xx} and T_{xy} respectively following the approach of Chanson and Carosi (2007) as well as the turbulence levels Tu of the aerated flows (Chanson and Toombes, 2002).

Further details about the experimental facility and the instrumentation can be found in Felder (2013).

2.2. Air–water flow patterns and properties

For a range of flow conditions (0.69 < d_c/h < 3.3), flow observations and detailed measurements of the air–water flow properties were conducted in transition flows (0.69 < d_c/h < 0.96) and skimming flows (0.96 < d_c/h < 3.3). The observations of flow patterns and flow properties were reported previously on the same stepped spillway facility and with the same double-tip conductivity probe as in the present study (Felder and Chanson, 2011, 2015). The results comprised detailed descriptions of flow patterns in transition and skimming flows (Felder and Chanson, 2015) as well as documentations of air–water flow properties including distributions of void fraction, bubble count rate, interfacial velocity, turbulence intensity and integral turbulent scales (Felder and Chanson, 2011, 2015).

Past observations of the air–water flow properties highlighted the special role of the intermediate flow region (30% < C < 70%) for strong air–water interfacial interactions including largest bubble count rates, turbulence levels and auto-and cross-correlation integral time scales as well as large transverse integral turbulent time and length scales (Felder and Chanson, 2015). For a central position within the intermediate flow region, i.e. C=0.5 +/− 0.01, the turbulence levels were about 100–140% and the time scales about 3.5–5.2 ms. The interfacial velocity exhibited a uniform profile in both intermediate flow region and spray region highlighting a close link between the interfacial velocities within the strongly aerated region above the bubbly flow region.

3. Characterization of air–water flows with 50% void fraction

To date, no attempt has been made to provide further insights into the air–water flow interactions within the intermediate flow region. In this section, the air–water flow interactions for the special case of equal liquid and void fractions are presented. Table 1 summarizes the flow conditions corresponding to C=50% +/− 1%. Table 1 lists also a number of characteristic air–water flow parameters including the depth averaged void fraction in a cross-section C_{mean}, the bubble count rate F_{50} and the interfacial velocity V_{50} for void fractions of C=50% +/− 1% as well as the maximum bubble count rate in a cross-section F_{max}.

The present data analyses focused upon the identification of characteristic time scales describing the air–water flow interactions within the bulk of the high-velocity flows. These time scales comprised the air bubble and droplet chord times and the interparticle arrival times. Further time scales were identified using spectral analyses of the instantaneous void fractions. The investigations comprised a range of flow conditions in both transition and skimming flows in the two stepped models. Only data were taken into consideration at locations at least three step edges downstream of the inception point of air entrainment to exclude data

Table 1
Experimental flow conditions and characteristic air–water flow parameters for the investigation of air–water flows with void fraction of $C = 0.50$ (+/− 0.01) on flat stepped spillways ($\theta = 26.6°$); double-tip conductivity probe data ($\varnothing = 0.25$ mm).

h [m]	d_c/h [-]	q_w [m^2/s]	Re [-]	Flow regime	Incep. point	C_{mean} [-]	Y_{90} [mm]	Step edge	C [-]	F_{50} [Hz]	V_{50} [m/s]	y [mm]	F_{max} [Hz]
0.1	0.69	0.056	2.2×10^5	TRA	3 to 4	0.558	56.8	7	0.492	191.7	2.72	22	202.8
	0.69	0.056	2.2×10^5	TRA	3 to 4	0.415	44.8	8	0.499	227.8	2.77	26	229.0
	1.11	0.116	4.6×10^5	SK	6	0.375	69.8	9	0.502	191.3	3.61	44	198.4
	1.28	0.143	5.7×10^5	SK	6 to 7	0.374	85.4	10	0.491	172.1	3.74	54	179.9
	1.28	0.143	5.7×10^5	SK	6 to 7	0.374	85.4	10	0.493	172.2	3.65	56	179.9
0.05	0.70	0.020	8.1×10^4	TRA	4	0.580	30.5	10	0.497	128.2	1.92	11	130.8
	0.70	0.020	8.1×10^4	TRA	4	0.521	24.8	13	0.502	138.2	1.97	11	138.2
	0.70	0.020	8.1×10^4	TRA	4	0.507	25.5	15	0.502	144.6	1.97	12	149.0
	0.70	0.020	8.1×10^4	TRA	4	0.527	26.7	16	0.505	145.7	2.00	12	148.2
	0.70	0.020	8.1×10^4	TRA	4	0.644	34.1	18	0.498	129.0	2.06	8	134.3
	1.14	0.042	1.7×10^5	SK	6 to 7	0.333	33.9	15	0.497	173.3	2.62	23	181.9
	1.14	0.042	1.7×10^5	SK	6 to 7	0.326	31.6	17	0.507	200.2	2.67	22	203.8
	1.66	0.075	3.0×10^5	SK	8 to 9	0.311	46.5	11	0.495	105.6	2.77	32	106.7
	1.66	0.075	3.0×10^5	SK	8 to 9	0.284	44.8	17	0.508	155.7	3.00	33	162.0
	1.66	0.075	3.0×10^5	SK	8 to 9	0.319	48.4	18	0.492	155.3	3.00	34	165.3
	2.22	0.116	4.6×10^5	SK	12	0.261	56.3	17	0.492	123.9	3.43	43	125.0
	2.22	0.116	4.6×10^5	SK	12	0.294	59.7	18	0.510	127.3	3.51	44	131.9
	2.22	0.116	4.6×10^5	SK	12	0.289	56.3	19	0.507	136.3	3.51	40	147.4

in the rapidly varied flows just downstream of the inception point (Table 1). Herein a variety of experimental configurations was used for the analyses of air–water flows with 50% void fraction.

3.1. Air bubble and water droplet chord times

For all flow conditions with $C = 50\%$ (+/− 1%), the air bubble and water droplet chord times were calculated providing a measure of the sizes of the air and water entities at a fixed position in a flow region with average void fraction of $C = 50\%$ +/− 1%. Typical probability distribution functions are illustrated in Fig. 2 allowing a direct comparison of sizes of air and water chords for the same flow conditions. The PDFs of air bubble and water droplet chord times indicated differences in chord sizes for positions with identical number of detected particles and identical void/liquid fractions. For all data, differences between the air bubble and water droplet chord times were observed with a larger amount of smaller air bubble chord sizes between 0–1 ms. The numbers of water droplet chord sizes were proportionally slightly larger for chord times between about 2–6 ms (Fig. 2).

Significant differences were also observed depending upon the characteristic bubble count rate F_{50} and step height h. The chord time distributions were regrouped into four different patterns (Fig. 2). For the stepped spillway with $h = 0.05$ m, three groups with similar bubble count rates were best suited (Fig. 2A–C) and the data for the steps with $h = 0.10$ m are illustrated in Fig. 2D for similar bubble count rates.

The finding of different probability functions for different bubble count rates (Fig. 2) suggested some link between the characteristic bubble count rate F_{50} and the mode of the chord time PDF distributions tch_{mode}. For all data, the relationship between F_{50} and tch_{mode} is illustrated in Fig. 3 for both step heights and for the air bubble and water droplet chord times. The observations indicated a monotonic decrease in the chord time mode with increasing bubble count rate (Fig. 3). Despite large data scatter, the present data trend was correlated by a power law:

$$tch_{\mathrm{mod}\,e} = 30.8 \times F_{50}^{-0.916} \quad (1)$$

Note that the number of data was limited and the inclusion of further data sets with 50% void fraction might provide more details about the relationship. The present results were comparable to limited observations by Toombes and Chanson (2008) at a single backward-facing step (Fig. 3). Toombes and Chanson (2007) used surface wave modeling to show the effects of surface waves upon the air bubble chord sizes. The differences between air bubble and water droplet chord times in the present study might also be linked with periodic variation of the pseudo-free-surface affecting the distribution of air–water interfaces in the intermediate flow region.

3.2. Inter-particle arrival times

For a dispersed phase, the analysis of inter-particle arrival times may provide some information on the randomness of the air–water structure and on preferential clustering for particular classes of particle sizes. Herein the inter-particle arrival times were analyzed for all measurement positions with $C = 50\%$ (+/− 1%) for five different chord time classes. Typical results are illustrated in Fig. 4 comprising both air bubble and water droplet PDFs. Little differences in the PDFs of the inter-particle arrival times were observed between bubble and droplet chord time distributions for all data and most chord time classes. For all present data, differences were however observed for the chord time classes 3–5 ms (Fig. 4D) which showed a larger number of smaller inter-particle arrival times for the water droplet chord times. The differences were associated with different numbers of air and water entities within this chord time class and

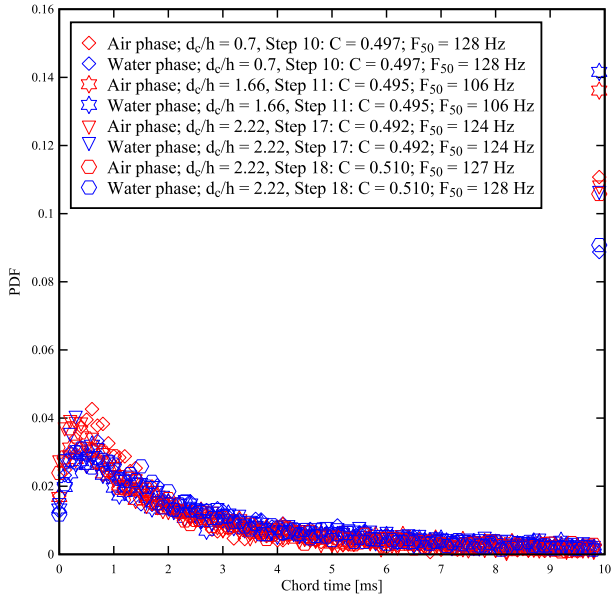

(A) Chord times for 100 Hz < F_{50} < 128 Hz; h = 5 cm

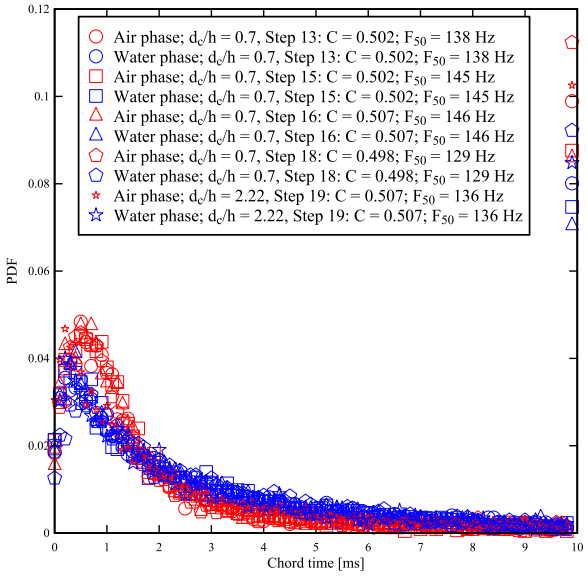

(B) Chord times for 129 Hz < F_{50} < 150 Hz; h = 5 cm

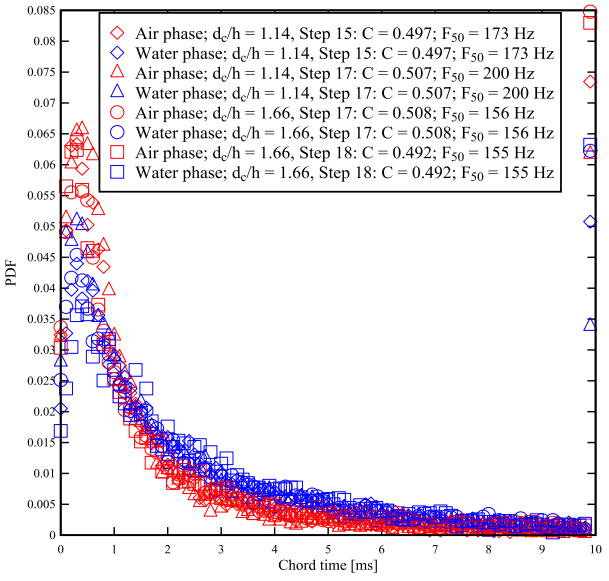

(C) Chord times for 150 Hz < F_{50} < 200 Hz; h = 5 cm

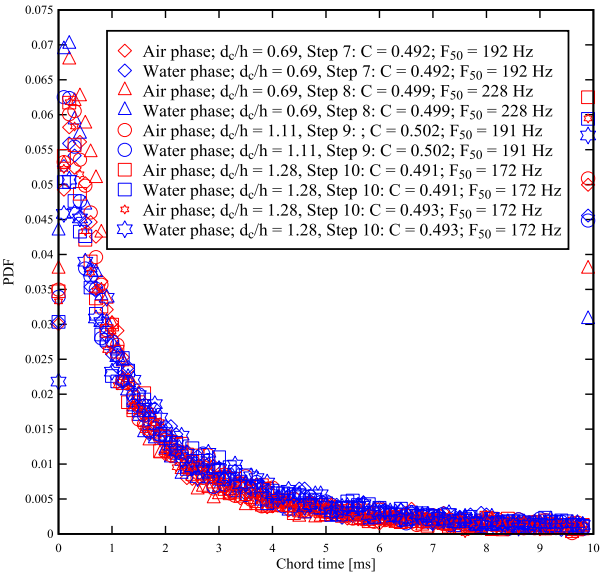

(D) Chord times for 170 Hz < F_{50} < 228 Hz; h = 10 cm

Fig. 2. Probability distribution functions of air bubble and water droplet chord times for void fractions of C=0.5 (+/− 0.01) in transition and skimming flows.

for all experiments, the number of bubble chords was about 40–60% of the number of droplet chords (Fig. 4D). For all other chord time classes, the numbers of bubbles and droplets were about the same.

These findings were observed for all data in transition and skimming flows and independent of the step heights. The shapes of the inter-particle arrival time distributions were affected by the number of particles in a chord time class. A larger number of particles resulted in a proportionally larger number of smaller inter-particle arrival times.

The reason for these differences for the chord time class 3–5 ms remains unknown. It is in agreement with the observations of a comparatively larger number of droplets with chord times of 2–6 ms (Fig. 2). The observations of the interparticle arrival time distributions for similar chord times were consistent with these findings. It appeared that the chord times of 3–5 ms might represent a characteristic time scale associated with the interaction of air bubbles and water droplets in the intermediate flow region. Interestingly the chord time scales were of similar magnitude compared to auto- and cross-correlation time scales and integral turbulent time scales observed in the intermediate flow region (Chanson and Carosi, 2007; Felder and Chanson, 2015). It is not known if there is a direct connection between the large size turbulent structures and the interparticle arrival times of bubble and droplet chords with chord sizes of 3–5 ms.

3.3. Spectral analyses of instantaneous void fractions

The instantaneous void fraction signal represented the streamwise distribution of air–water interfaces at the fixed position of the conductivity probe's leading tip. A spectral analysis was conducted for the instantaneous signals to identify characteristic

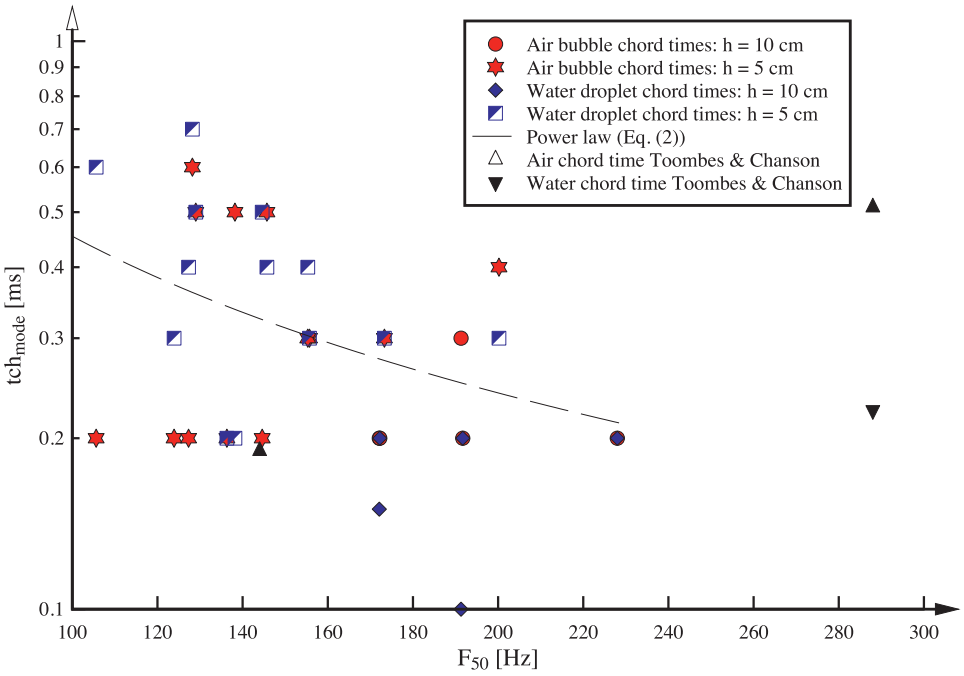

Fig. 3. Dimensionless relationship between mode of the chord time PDF and characteristic bubble count rate F_{50}; comparison with best-fit correlation (Eq. (1)) and data by Toombes and Chanson (2008).

frequencies associated with the air–water flows with $C = 50\%$ (+/− 1%). For each data set, an FFT analysis was conducted for 13 non-overlapping intervals of 65,536 (= 2^{16}) points and the results were averaged (Fig. 5). The ensemble averaging allowed an easier identification of the characteristic frequencies due to a strong scatter of data. Further sensitivity analyses were conducted using several filter and smoothing techniques. Little effects on the characteristic frequencies were observed and the ensemble averaging of 13 non-overlapping instantaneous void fraction components was considered suitable.

Fig. 5 illustrates typical power spectrum density functions of the instantaneous void fractions for transition and skimming flows, both step heights and $C = 50\%$ (+/− 1%). In Fig. 5, the black curves illustrate the ensemble averaged data. All curves showed a range of characteristic frequencies between 0.9 and 100 Hz with various peaks within this frequency range (Fig. 5). For all data sets, all dominant characteristic frequencies and the corresponding power spectrum density (PSD) were recorded. The present results differed substantially to observations in the bubbly flow region investigated for a similarly sloped stepped chute by Gonzalez (2005).

The characteristic frequencies for all data sets are summarized in Fig. 6 as a function of the corresponding PSD maxima. The observations for all experiments showed consistent results as illustrated by the median curve (Fig. 6). It appeared that a distinctive frequency of about 9–10 Hz was representative for air–water flows with $C = 50\%$ (+/− 1%). Similar characteristic frequencies were observed in probability distribution functions of the PSD values with bin sizes of 1 Hz and 3 Hz respectively (Fig. 7).

The present observation was significant since the characteristic frequencies observed in the PSDs identified a range of dominant time scales of the air–water interactions within the intermediate flow region for $C = 50\%$ (+/− 1%). The results indicated a wide range of characteristic frequencies within 2 to 100 Hz, with a distinctive frequency of about 9–10 Hz. That is, the interactions between the air–water interfaces were most energetic with relatively slow fluctuating processes with a time scale of about 0.1 s. With increasing frequency, and decreasing time scale, the PSD function maxima decreased monotonically (Fig. 6) indicating a smaller contribution of the fast fluctuating interactions of the air–water interfaces. The PSD density function for frequencies smaller about 10 Hz showed a decrease in PSD maxima with decreasing frequency.

Overall, the air–water interactions in the intermediate flow region were mostly characterized by relatively slow fluctuating processes, rather than very fast, rapid interactions between air bubbles and water droplets. The most energetic time scales were comparatively slow.

The characteristic time scale in the intermediate flow region of about 0.1 s was used for the calculation of the corresponding length scale using two different characteristic velocities, i.e. the interfacial velocity V_{50} and the free-surface celerity C_S. The interfacial velocity V_{50} was measured with a double-tip conductivity probe and the characteristic values are listed in Table 1. The free-surface celerity was calculated based upon the characteristic flow depth Y_{90} as a representative value of the air–water free-surface depth:

$$C_S = \sqrt{g \times Y_{90}} \quad (2)$$

For the present data set, the resulting length scales were in the order of 200–350 mm calculated with the interfacial velocity V_{50} and in a range of about 50–100 mm for the free-surface celerity C_S. These length scales were significantly larger than scales linked with the millimetric and sub-millimetric processes in the intermediate flow region. They were in a similar order of magnitude as the step heights, the cavity length and the air–water flow depths.

4. Discussion

The analysis of instantaneous void fraction data with $C = 50\%$ (+/-1%) highlighted a number of air–water time scales characterizing the interactions between air–water interfaces. Table 2 summarizes these characteristic time scales (upper half), while further time scales observed on the same stepped spillway models are also listed (middle section). In the lower part of Table 2, several other time scales for high-velocity air–water flows are listed for comparison.

The present findings identified chord times of 3–5 ms in the intermediate flow region which might represent a characteristic

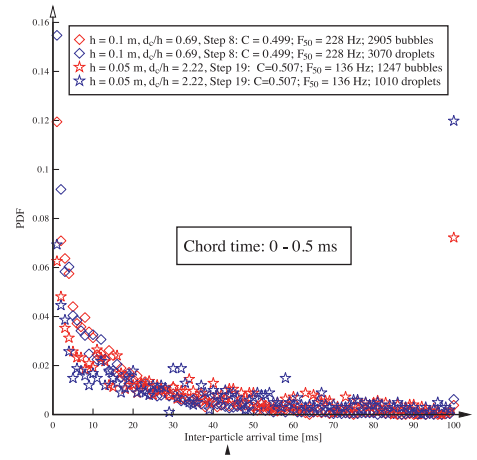

(A) Chord time class: 0 – 0.5 ms

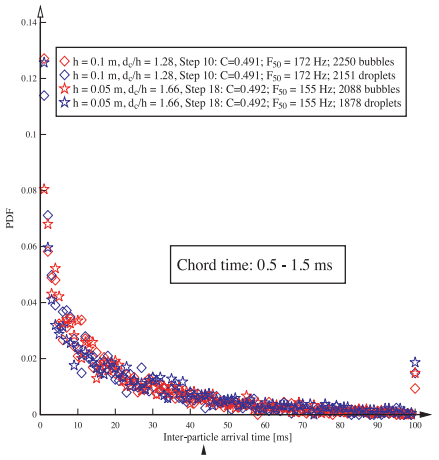

(B) Chord time class: 0.5 – 1.5 ms

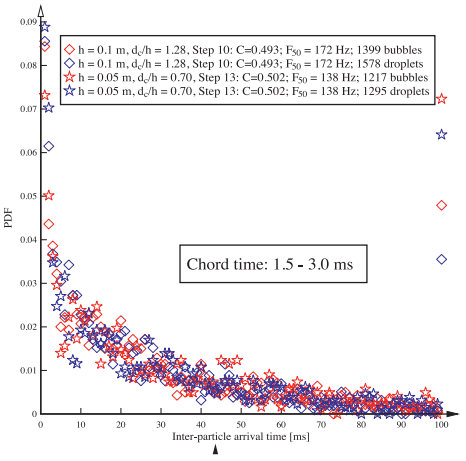

(C) Chord time class: 1.5 – 3.0 ms

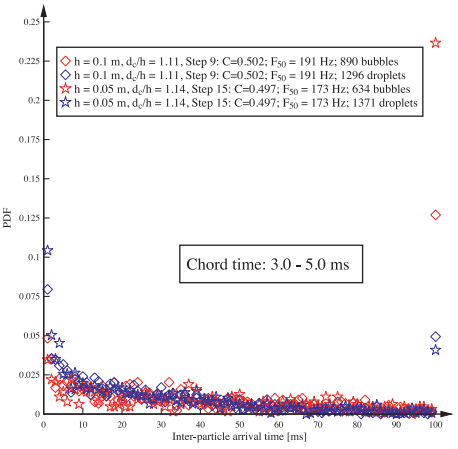

(D) Chord time class: 3.0 – 5.0 ms

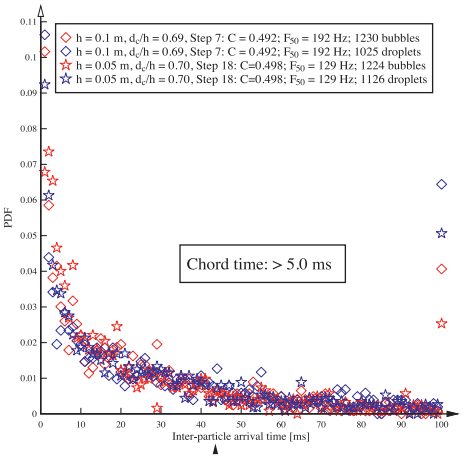

(E) Chord time class: > 5.0 ms

Fig. 4. Inter-particle arrival times for different air bubble and water droplet chord time classes for void fractions of $C \approx 50\%$ in transition and skimming flows on flat stepped spillways ($\theta = 26.6°$).

time scale associated with the interaction of air and water entities in the intermediate flow region. Such time scales were of similar magnitude as the auto- and cross-correlation time scales and integral turbulent time scales observed in the intermediate flow region (Felder and Chanson, 2015). The time scales were also similar to time scales associated with bubble break up processes in aerated flows (Table 2). Available data in the literature suggested a range of typical break-up time scales from 1.3 ms (Chanson and Cummings, 1992), 8.5–11.8 ms (Hinze, 1955; Sevik and Park, 1973; Gulliver et al., 1990), to 20 ms (Cummings and Chanson, 1999). While the differences in bubble break-up scales must be acknowledged, it is important to notice that the time scales associated with the break-up processes are of similar magnitude compared to the characteristic time scales in the intermediate flow region. A further similar time scale linked with turbulent velocity fluctuations was also very close (Ervine and Falvey, 1987). The agreement of

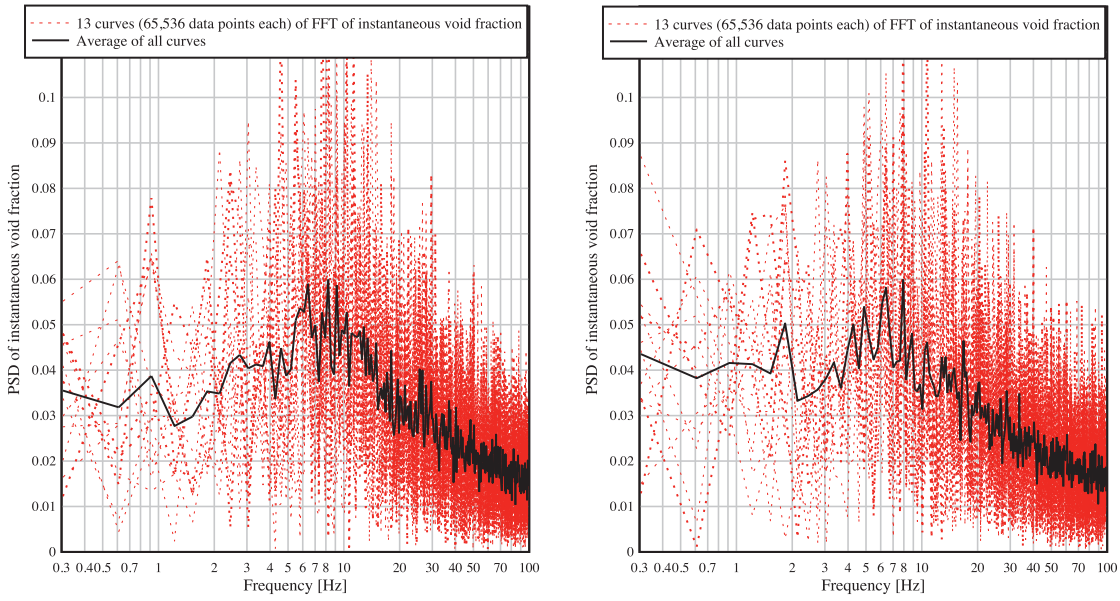

(A) TRA: $d_c/h = 0.70$; $q_w = 0.020$ m^2/s; Re = 8.1×10^4 Step 16; h = 5 cm: C = 0.505, F_{50} = 145.7 Hz

(B) SK: $d_c/h = 1.11$; $q_w = 0.116$ m^2/s; Re = 4.6×10^5; Step 9; h = 10 cm: C = 0.502, F_{50} = 191.3 Hz

Fig. 5. Spectral analysis of the instantaneous void fraction signal for void fractions of $C \approx 50\%$ in transition and skimming flows; Conductivity probe signal (Ø = 0.25 mm); sampling time 45 s, sampling frequency 20 kHz.

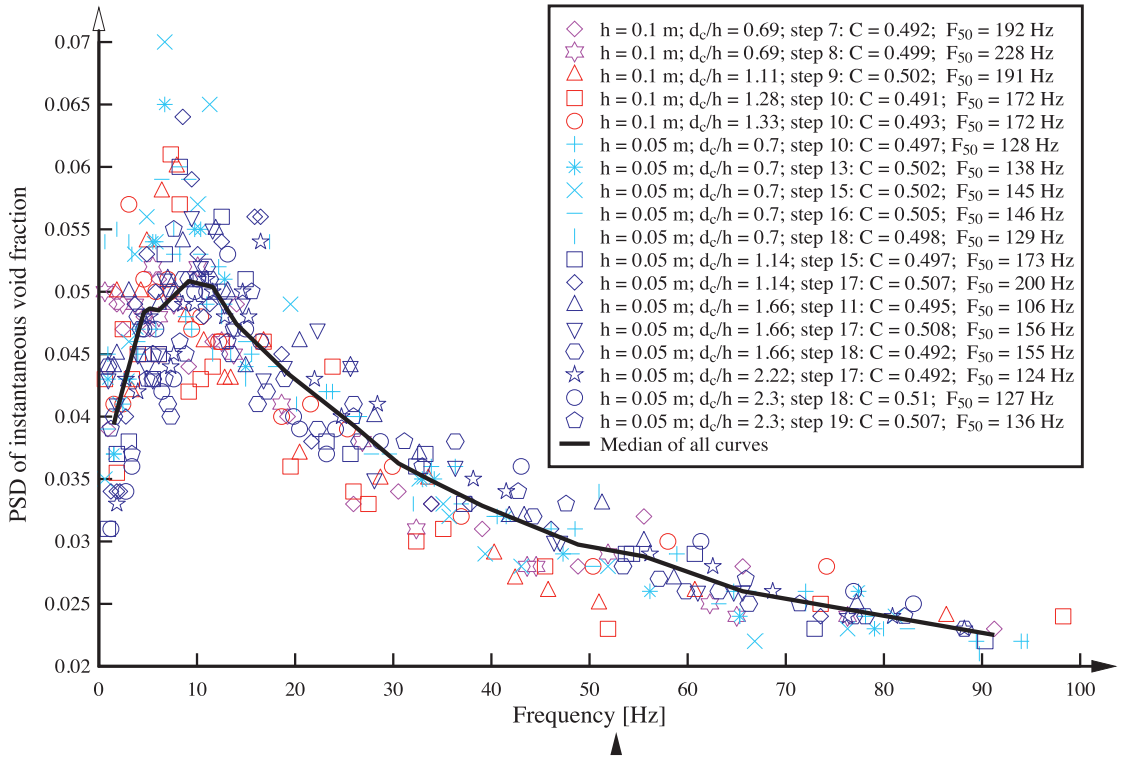

Fig. 6. Summary of characteristic frequencies and corresponding power spectrum densities (PSD) of the instantaneous void fraction signals for void fractions of $C \approx 50\%$ in transition and skimming flows on flat stepped spillways.

characteristic chord times and integral turbulent scales for $C = 50\%$ (+/− 1%) with time scales associated with bubble break up and turbulent velocity fluctuations suggested a close link between turbulence properties and sizes of air–water entities.

The spectral analyses of instantaneous void fractions identified a range of characteristic frequencies between 2 and 100 Hz, independently of flow regime and of step heights, for $C = 50\%$ (+/− 1%). Frequencies of 10 Hz were the most energetic frequencies, corresponding to a time scale of 0.1 s. This time scale was two orders of magnitude larger than the characteristic integral turbulent time scales within the intermediate flow region. In other words, the characteristic time scale of instantaneous void fraction signal

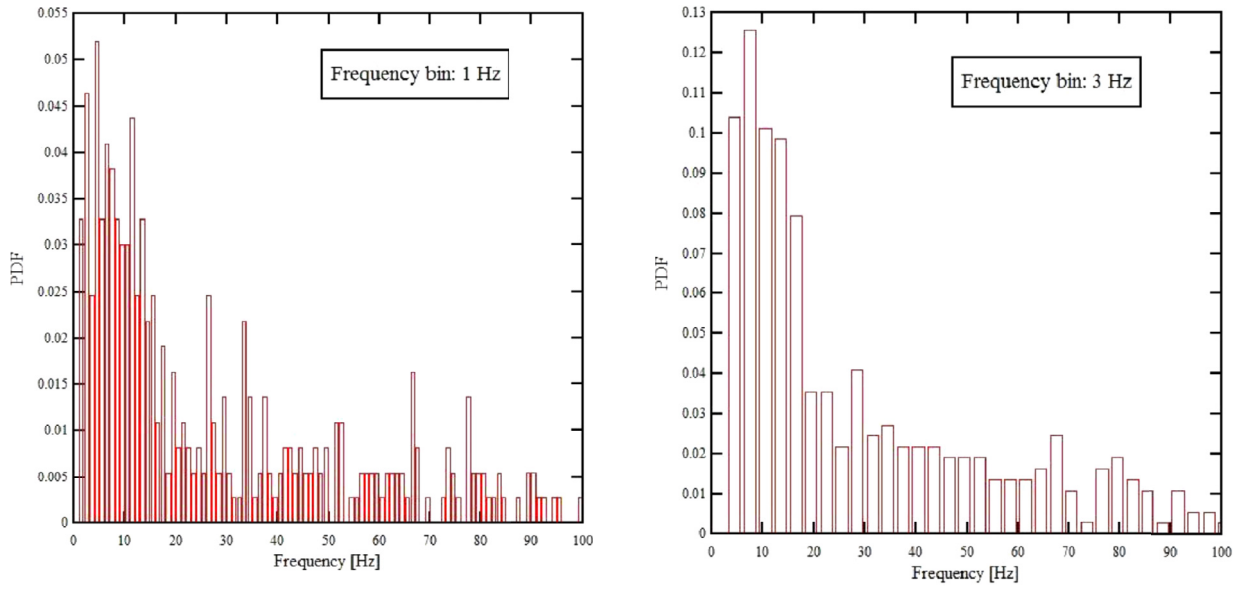

(A) Bin size of frequency: 1 Hz (B) Bin size of frequency: 3 Hz

Fig. 7. PDF of characteristic frequencies of the instantaneous void fraction signals for void fractions of $C \approx 50\%$ in transition and skimming flows.

Table 2
Summary of characteristic time scales in the intermediate flow region ($C = 0.50$ (+/− 0.01)). Air–water flow measurements on flat stepped spillways with $\theta = 26.6°$.

Time scale [ms]	Comment	Section/reference
3–5	Differences in inter-particle arrival times for air bubble and water droplets ($C = 0.50$ (+/− 0.01))	Section 3.2
100	Time scale based upon FFT analysis of instantaneous void fraction ($C = 0.50$ (+/− 0.01))	Section 3.3
3.5–5.2	Maximum auto- and cross-correlation time scales in a cross-section for a double-tip conductivity probes ($0.3 < C < 0.7$)	Felder (2013), Felder and Chanson (2015)
3–4	Maximum integral turbulent time and length scales in a cross-section for an array of two single-tip conductivity probes for ($0.3 < C < 0.7$)	Felder (2013), Felder and Chanson (2015)
50–200	Free-surface auto-correlation time scales in the air–water flow region ($C > 0.7$)	Felder (2013), Felder and Chanson (2014)
1000–5000	Time scales based upon visual observations of characteristic cavity ejection frequencies ($C < 0.3$)	Guenther et al. (2013)
8.5–11.8	Bubble break-up time scales	Hinze (1955), Sevik and Park (1973), Gulliver et al. (1990)
1.3	Bubble break-up time scales	Chanson and Cummings (1992)
3.6	Time scales linked with turbulent velocity fluctuations	Ervine and Falvey (1987)
20	Bubble break-up time scale in vertical supported jets	Cummings and Chanson (1999)

was possibly linked to large scale free-surface fluctuations rather than to the air−water interactions on a sub-millimetric level. Free-surface measurements with acoustic displacement meters in the aerated flow region identified free-surface auto-correlation time scales of a similar order of magnitude of about 0.05–0.2 s (Bung, 2013; Felder and Chanson, 2014). It is believed that this agreement confirmed some coupling between vertical free-surface motion and air–water flow properties, as reported previously (Killen, 1968; Wilhelms and Gulliver, 2005; Toombes and Chanson, 2007, 2008).

In contrast, cavity ejection frequencies were investigated on a stepped spillway with $\theta = 26.6°$ (Guenther et al., 2013). The characteristic cavity ejection frequencies were about 0.2–1 Hz. They differed from the characteristic frequencies in the intermediate flow region, indicating that the cavity ejection processes did not impact upon the air–water flow structure in the intermediate flow region.

5. Conclusion

Air–water flow experiments were conducted in high-velocity free-surface flows on a stepped spillway, with a focus on the detailed air–water interactions in the flow region with same amount of air and water phases: i.e., $C = 50\%$ (+/− 1%). The data comprised a range of flow conditions in both transition and skimming flows for two step heights. Several processing techniques of the instantaneous void fraction signal provided estimates of characteristic time scales. The comparison of air bubble and water droplet chord time distributions showed a larger number of smaller air chord times and a larger number of water chords with times of 2–6 ms. An interparticle arrival time analysis identified particle chord times of 3–5 ms as a representative characteristic time scale associated with the interaction between air–water and water–air interfaces in the intermediate flow region. Such time scales were of similar magnitude to the auto- and cross-correlation time scales, to integral turbulent time scales and to time scales associated with bubble break up and turbulent velocity fluctuations. A distinctive frequency of about 10 Hz was identified using spectral analyses of the instantaneous void fraction signals. The corresponding time scale of 0.1 s appeared to be linked with large scale free-surface fluctuations. Such a magnitude was similar to free-surface auto-correlation time scales indicating that the air–water flow structure might be affected by free-surface waves. While the present results provided first in-depth insights into the characteristics of flows with equal entities of air and water, the air–water flow processes within the intermediate flow region remain poorly understood and further research is needed.

Acknowledgments

The financial support of the Australian Research Council (Grants DP0818922 and DP120100481) is acknowledged.

References

Bung, D.B., 2011. Developing flow in skimming flow regime on embankment stepped spillways. J. Hydraul. Res. IAHR 49 (5), 639–648. doi:10.1080/00221686.2011.584372.

Bung, D.B., 2013. Non-intrusive detection of air–water surface roughness in self-aerated chute flows. J. Hydraul. Res. IAHR 51 (3), 322–329. doi:10.1080/00221686.2013.777373.

Cartellier, A., Achard, J.L., 1991. Local phase detection probes in fluid/fluid two-phase flows. Rev. Sci. Instrum. 62, 279–303.

Chanson, H., 1997. Air Bubble Entrainment in Free-Surface Turbulent Shear Flows. Academic Press, London, UK, p. 401.

Chanson, H., 2013. Hydraulics of aerated flows: Qui Pro Quo? J. Hydraul. Res. IAHR 51 (3), 223–243. doi:10.1080/00221686.2013.795917, Invited Vision paper.

Chanson, H., Carosi, G., 2007. Advanced post-processing and correlation analyses in high-velocity air-water flows. Environ. Fluid Mech. 5, 495–508. doi:10.1007/s10652-007-9038.

Chanson, H., and Cummings, P.D. (1992). "Aeration of the Ocean due to Plunging Breaking Waves.Research Report No. CE142, Dept. of Civil Engineering, University of Queensland, Australia, Nov., 42 pages (ISBN 0 86776 502 X).

Chanson, H., Toombes, L., 2002. Air-water flows down stepped chutes: turbulence and flow structure observations. Int. J. Multiph. Flow 27 (11), 1737–1761.

Crowe, C., Sommerfield, M., Tsuji, Y., 1998. Multiphase Flows with Droplets and Particles. CRC Press, Boca Raton, USA, p. 471.

Cummings, P.D., Chanson, H., 1999. An experimental study of individual air bubble entrainment at a planar plunging jet. Chem. Eng. Res. Des. Trans. IChemE Part A 77 (A2), 159–164.

Edward, C.F., Marx, K.D., 1995. Multipoint statistical structure of the ideal spray, part ii: evaluating steadiness using the interparticle time distribution. At. Sprays 5, 435–455.

Ervine, D.A., 1998. Air entrainment in hydraulic structures: a review. Proc. Inst. Civ. Eng. Water Marit. Energy 130, 142–153.

Ervine, D.A., Falvey, H.T., 1987. Behaviour of turbulent water jets in the atmosphere and in plunge pools. Proc. Inst. Civ. Eng. Lond. Part 2 83, 295–314.

Felder, S. (2013). "Air-Water Flow Properties on Stepped Spillways for Embankment Dams: Aeration, Energy Dissipation and Turbulence on Uniform, Non-Uniform and Pooled Stepped Chutes." Ph.D. thesis, School of Civil Engineering, The University of Queensland, Brisbane, Australia

Felder, S., Chanson, H., 2011. Air-water flow properties in step cavity down a stepped chute. Int. J. Multiph. Flow 37 (7), 732–745. doi:10.1016/j.ijmultiphaseflow.2011.02.009.

Felder, S., Chanson, H., 2014. Air–water flows and free-surface profiles on a non-uniform stepped chute. J. Hydraul. Res. 52, 253–263. doi:10.1080/00221686.2013.841780.

Felder, S., Chanson, H., 2015. Phase-detection probe measurements in high-velocity free-surface flows including a discussion of key sampling parameters. Exp. Therm. Fluid Sci. 61, 66–78. doi:10.1016/j.expthermflusci.2014.10.009.

Gonzalez, C.A. (2005). "An Experimental Study of Free-Surface Aeration on Embankment Stepped Chutes", Ph.D. thesis, University of Queensland, Australia.

Guenther, P., Felder, S., Chanson, H., 2013. Flow aeration, cavity processes and energy dissipation on flat and pooled stepped spillways for embankments. Environ. Fluid Mech. 13, 503–525. doi:10.1007/s10652-013-9277-4.

Gulliver, J.S., Thene, J.R., Rindels, A.J., 1990. Indexing gas transfer in self-aerated flows. J. Environ. Eng. ASCE 116 (3), 503–523.

Hinze, J., 1955. Fundamentals of hydrodynamic mechanism of splitting in dispersion process. AIChE J. 1 (3), 289–295.

Hoyt, J.W., Sellin, R.H.J., 1989. Hydraulic jump as 'mixing layer'. J. Hydraul. Eng. ASCE 115 (12), 1607–1614.

Hoyt, J.W., Taylor, J.J., 1976. Mechanism of air entrainment in a high speed water jet. In: Proceedings of the IAHR/SHF Symposium. Grenoble, France, pp. 329–335.

Killen, J.M. (1968). "The Surface Characteristics of Self-Aerated Flow in Steep Channels." Ph.D. thesis, University of Minnesota, Minneapolis, USA.

Kobus, H., 1984. Symposium on scale effects in modelling hydraulic structures. In: Proceedings of the IAHR World Congress. Esslingen, Germany.

McKeogh, E.J., Ervine, D.A., 1981. Air entrainment rate and diffusion pattern of plunging liquid jets. Chem. Eng. Sci. 36, 1161–1172.

Matos, J. (1999). "Emulsionamento de ar e Dissipação De Energia do Escoamento em Descarregadores em Degraus." ('Air entrainment and energy dissipation in flow over stepped spillways.') Ph.D. thesis, IST, Lisbon, Portugal (in Portuguese).

Ohtsu, I., Yasuda, Y., Takahashi, M., 2004. Flow characteristics of skimming flows in stepped channels. J. Hydraul. Eng. ASCE 130 (9), 860–869.

Rao, N.S.L., Kobus, H.E., 1971. Characteristics of self-aerated free-surface flows. Water Waste Water/Current Research and Practice, 10. Eric Schmidt Verlag, Berlin.

Sevik, M., Park, S.H., 1973. The splitting of drops and bubbles by turbulent fluid flow. J. Fluids Eng. ASME 95, 53–60.

Straub, L.G., Anderson, A.G., 1958. Experiments on self-aerated flow in open channels. J. Hydraul. Div. Proc. ASCE 84 (HY7) paper 1890, 1–35.

Thomas, R.M., 1981. Bubble coalescence in turbulent flows. Int. J. Multiph. Flow 7 (6), 709–717.

Toombes, L., Chanson, H., 2007. Surface waves and roughness in self-aerated supercritical flow. Environ. Fluid Mech. 7 (3), 259–270. doi:10.1007/s10652-007-9022-y.

Toombes, L., Chanson, H., 2008. Interfacial aeration and bubble count rate distributions in a supercritical flow past a backward-facing step. Int. J. Multiph. Flow 34 (5), 427–436 (doi.org/10.1016/j.ijmultiphaseflow.2008.01.005).

Wilhelms, S.C., Gulliver, J.S., 2005. Bubbles and waves description of self-aerated spillway flow. J. Hydraul. Res. 43, 522–531.

Wood, I.R., 1991. Air entrainment in free-surface flows. IAHR Hydraulic Structures Design Manual, 4. Balkema Publ., Rotterdam.

Wu, P.K., Tseng, L.K., Faeth, G.M., 1992. Primary breakup in gas/liquid mixing layers for turbulent liquids. At. Sprays 2, 295–317.